Supporting Information for

Use of 2,3,5-F_3Y-β2 and 3-NH_2Y-α2 to study PCET in *E. coli* Ribonucleotide Reductase

Mohammad R. Seyedsayamdost,[†,&] Cyril S. Yee,[†] and JoAnne Stubbe*[,†,‡]

Department of Chemistry[†] and Biology[‡], Massachusetts Institute of Technology, 77 Massachusetts Avenue, Cambridge, MA 02139–4307

[&]*Current address: Department of Biological Chemistry and Molecular Pharmacology, 240 Longwood Avenue, C1-609, Boston, MA 02115*

* To whom correspondence should be addressed. Tel: (617) 253-1814. Fax: (617) 258-7247. E-mail: stubbe@mit.edu

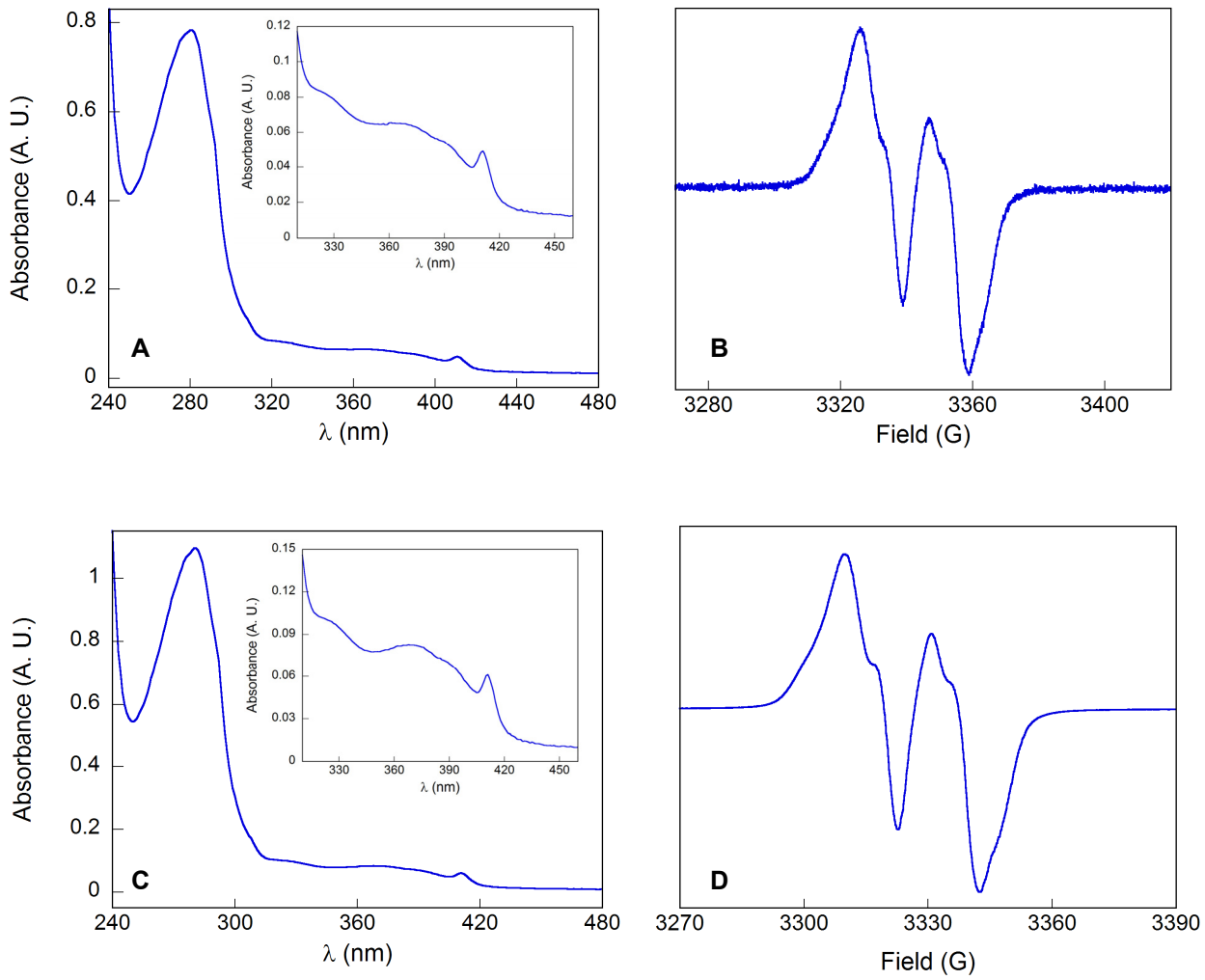

Figure S1: Increasing the radical content of intein wt-β2 and F_3Y_{356}-β2. UV-vis (A) and EPR (B) spectra of intein wt-β2 (1.1 Y_{122}•/dimer) after the chelation/reconstitution procedure. The inset (A) is a magnified view of the features associated with the Y_{122}• diiron cluster. UV-vis (C) and EPR (D) spectra of F_3Y_{356}-β2 (1.2 Y_{122}•/dimer) after the chelation/reconstitution procedure. The inset (C) shows a magnified view of the features associated with the Y_{122}• diiron cluster.

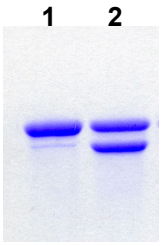

Figure S2: SDS PAGE analysis of F_3Y_{356}-β2 (lane 1, 4 μg) and F_3Y_{356}-ββ' (lane 2, 4 μg) after the chelation/reconstitution procedure.

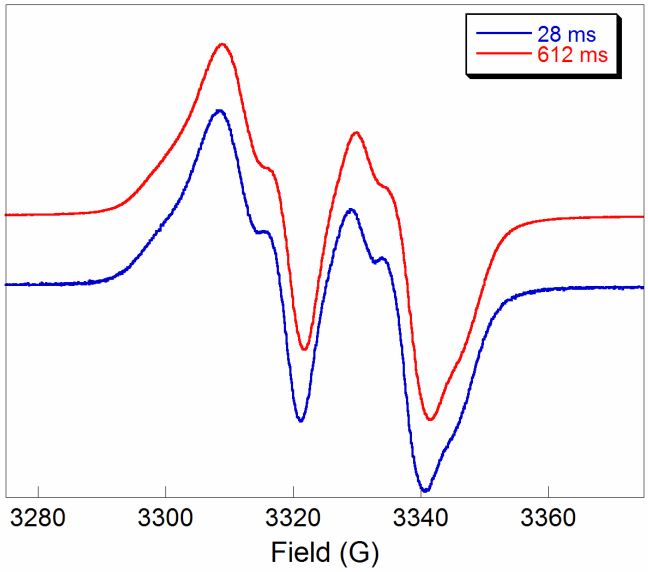

Figure S3: EPR spectra of the reaction of F_3Y_{356}-β2 with wt α2 in the presence of CDP/ATP quenched after 28 ms and 612 ms. The spectra were recorded at 77 K.

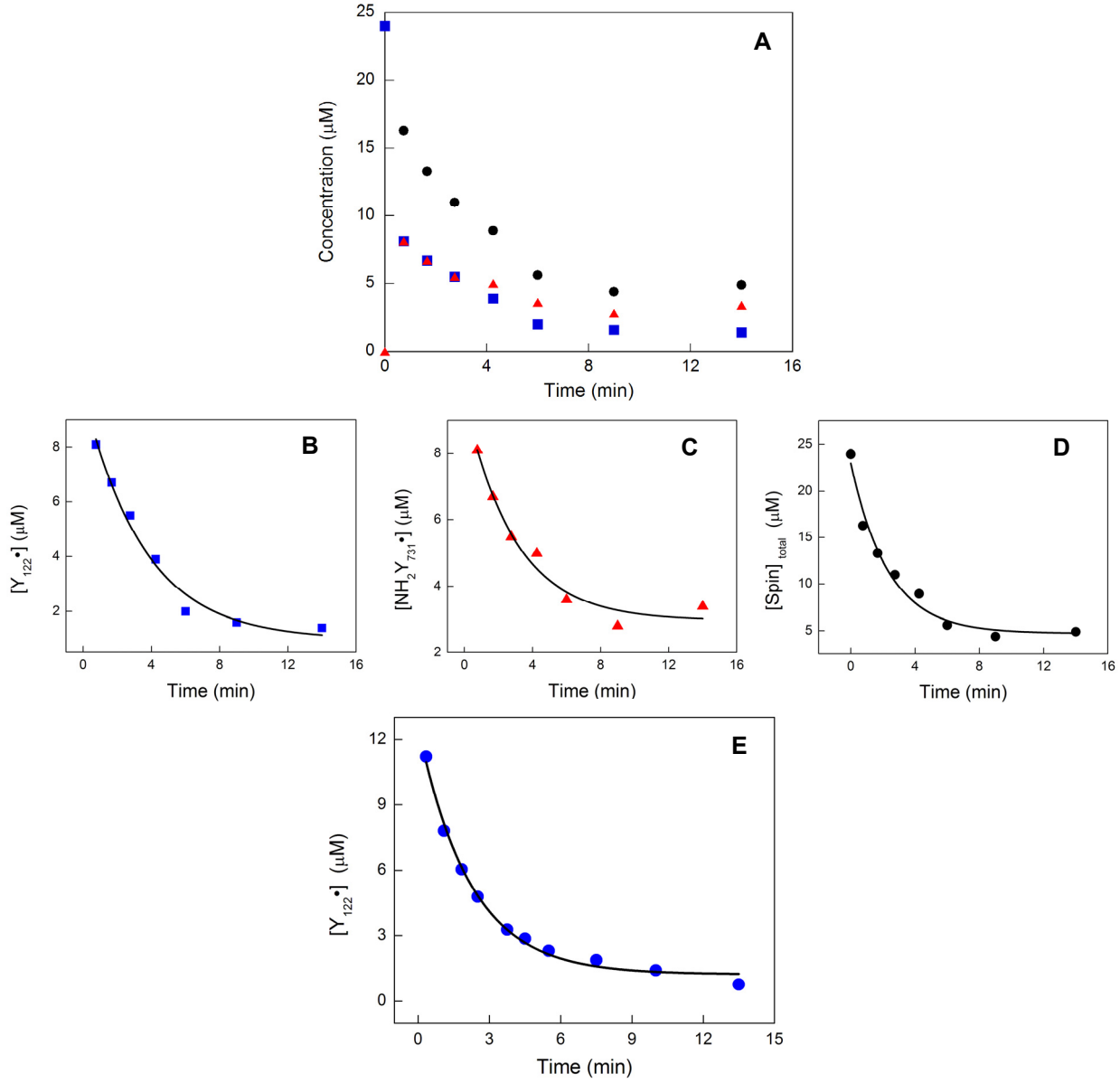

Figure S4: Stability of NH_2Y_{731}• probed by EPR and UV-vis spectroscopy. (A) NH_2Y_{731}-α2 and ATP were mixed with wt β2 (1.2 Y_{122}• / β2) and CDP at 25°C to give final concentrations of 20 μM, 3 mM, 20 μM and 1 mM, respectively. At defined time points, an aliquot was removed, transferred to an EPR tube, frozen in liquid N_2 and its EPR spectrum recorded. (B-E) The analysis and fits for the data in panel (A) are shown in panels B-E. For each time point, the $[spin]_{total}$ (black dots) and its distribution between Y_{122}• (blue squares) and NH_2Y_{731}• (red triangles) was determined and plotted vs. time. Time courses for [Y_{122}•] (B), [NH_2Y_{731}•] (C), and $[spin]_{total}$ (D) are shown with mono-exponential fits to the data indicated by black lines. (E) Time course of Y_{122}• decay measured by UV–vis spectroscopy. The reaction was carried out at 25°C and contained final concentrations of 18 μM NH_2Y_{731}-α2/β2 (1.2 Y_{122}• / β2) and 1 mM CDP and 3 mM ATP. At defined time points a UV-vis spectrum was recorded and the [Y_{122}•] (blue dots) computed using the dropline method. The black line is a mono-exponential fit to the data. The fits above yield decay rate constants 0.0057 ± 0.0013 s^{-1} for Y_{122}• (B), 0.0052 ± 0.0017 s^{-1} for NH_2Y_{731}• (C), 0.0072 ± 0.0012 s^{-1} for $[spin]_{total}$ (D), and 0.0065 ± 0.0005 s^{-1} for Y_{122}• determined by UV-vis spectroscopy (E), giving an average decay *k* of 0.0062 ± 0.0012 s^{-1}.

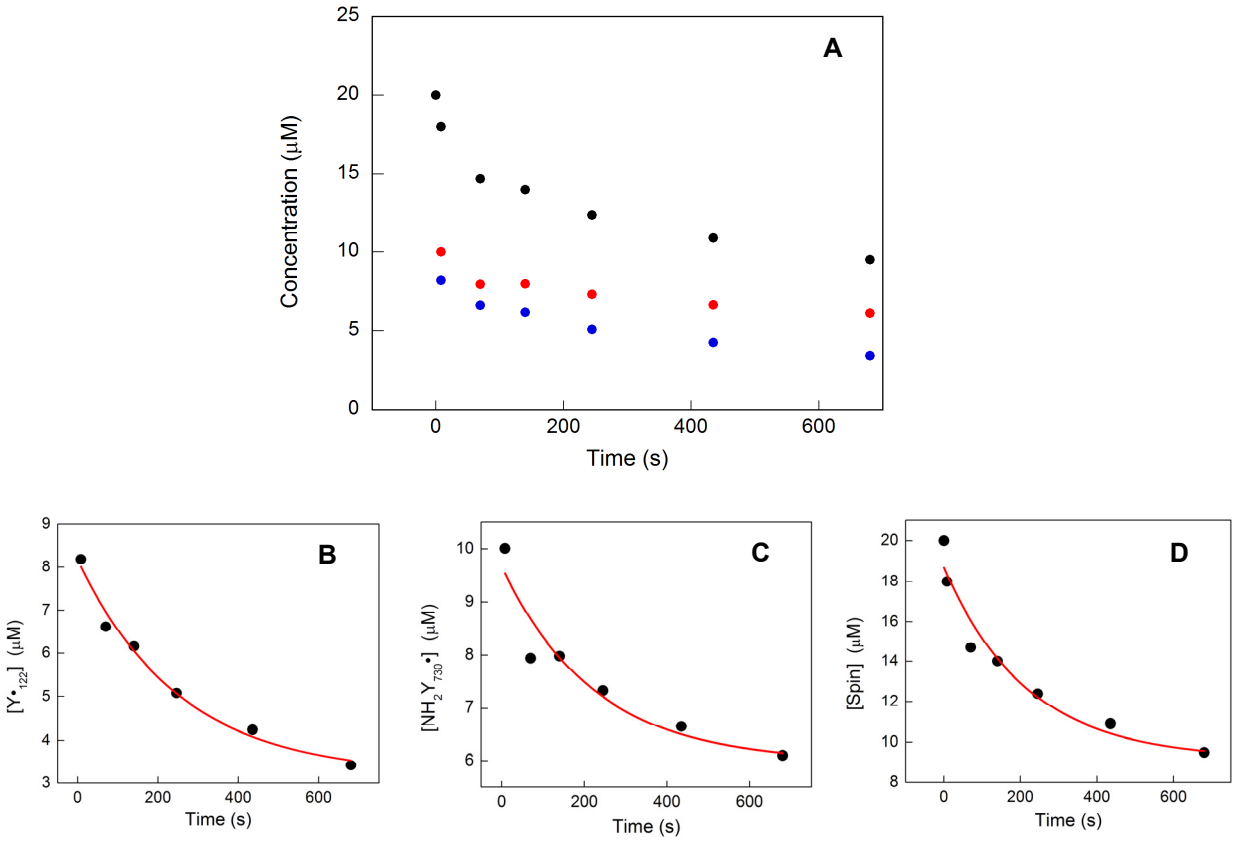

Figure S5: Stability of NH_2Y_{730}• probed by EPR spectroscopy. (A) NH_2Y_{730}-α2 and ATP were mixed with wt β2 (1.0 Y_{122}• / β2) and CDP at 25°C to give final concentrations of 20 μM, 3 mM, 20 μM and 1 mM, respectively. At defined time points, an aliquot was removed, transferred to an EPR tube, frozen in liquid N_2 and its EPR spectrum recorded. (B-D) The analysis and fits for the data in panel (A) are shown in panels B-D. For each time point, the $[spin]_{total}$ (black dots) and its distribution between Y_{122}• (blue squares) and NH_2Y_{730}• (red triangles) was determined and plotted vs. time. Time courses for [Y_{122}•] (B), [NH_2Y_{730}•] (C), and $[spin]_{total}$ (D) are shown with mono-exponential fits to the data indicated by red lines yielding rate constants of 0.004 ± 0.00083 s^{-1} (B) and 0.0043 ± 0.0015 s^{-1} (C) and 0.0045 ± 0.0011 s^{-1} (D), giving an average rate constant of 0.0043 ± 0.0011 s^{-1}.

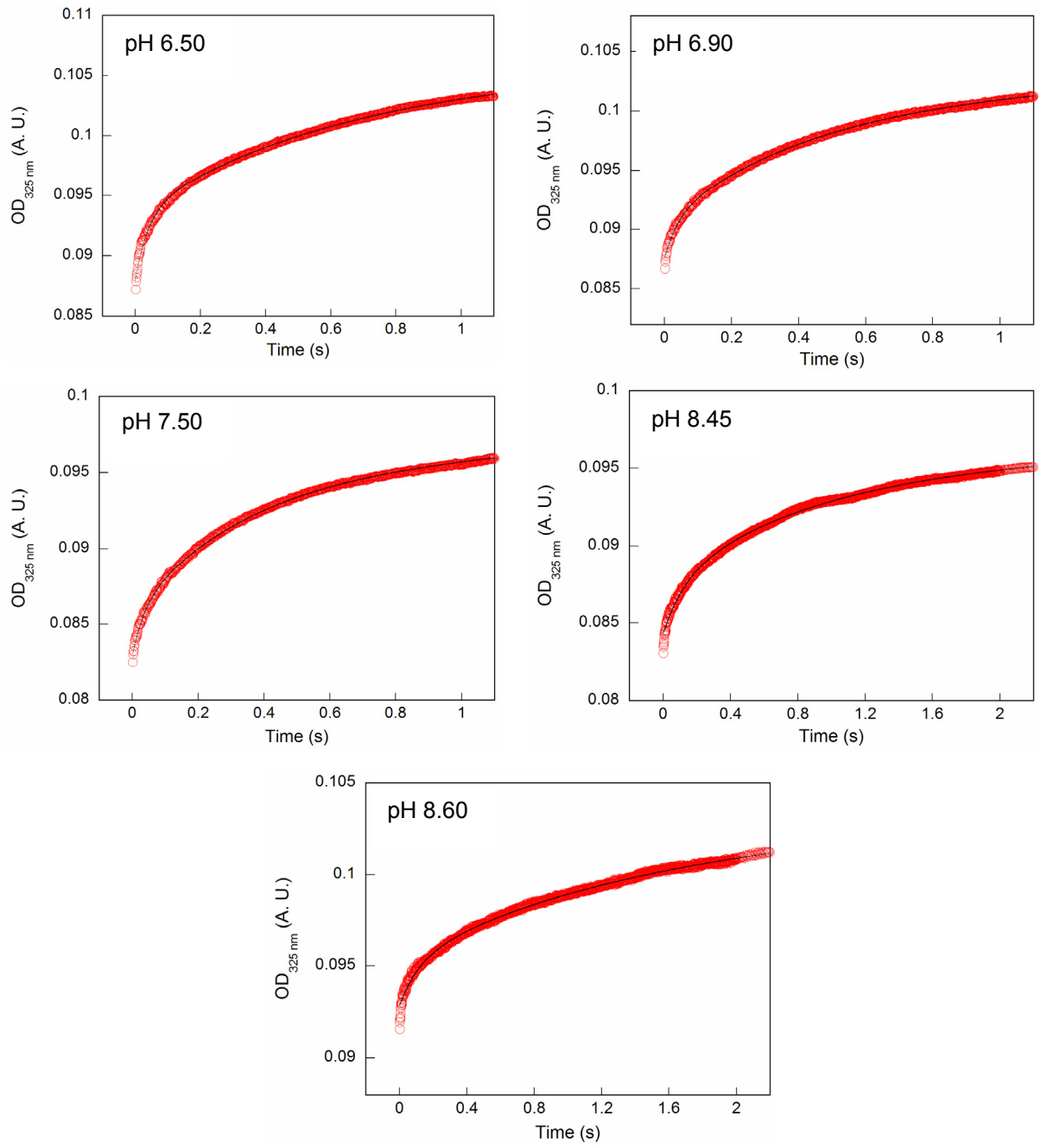

Figure S6: Magnified view of the initial 1-2 s of the SF UV-vis traces shown in Fig. 3 for the reaction of NH_2Y_{731}-α2 with F_3Y_{356}-β2 in the presence of CDP/ATP.

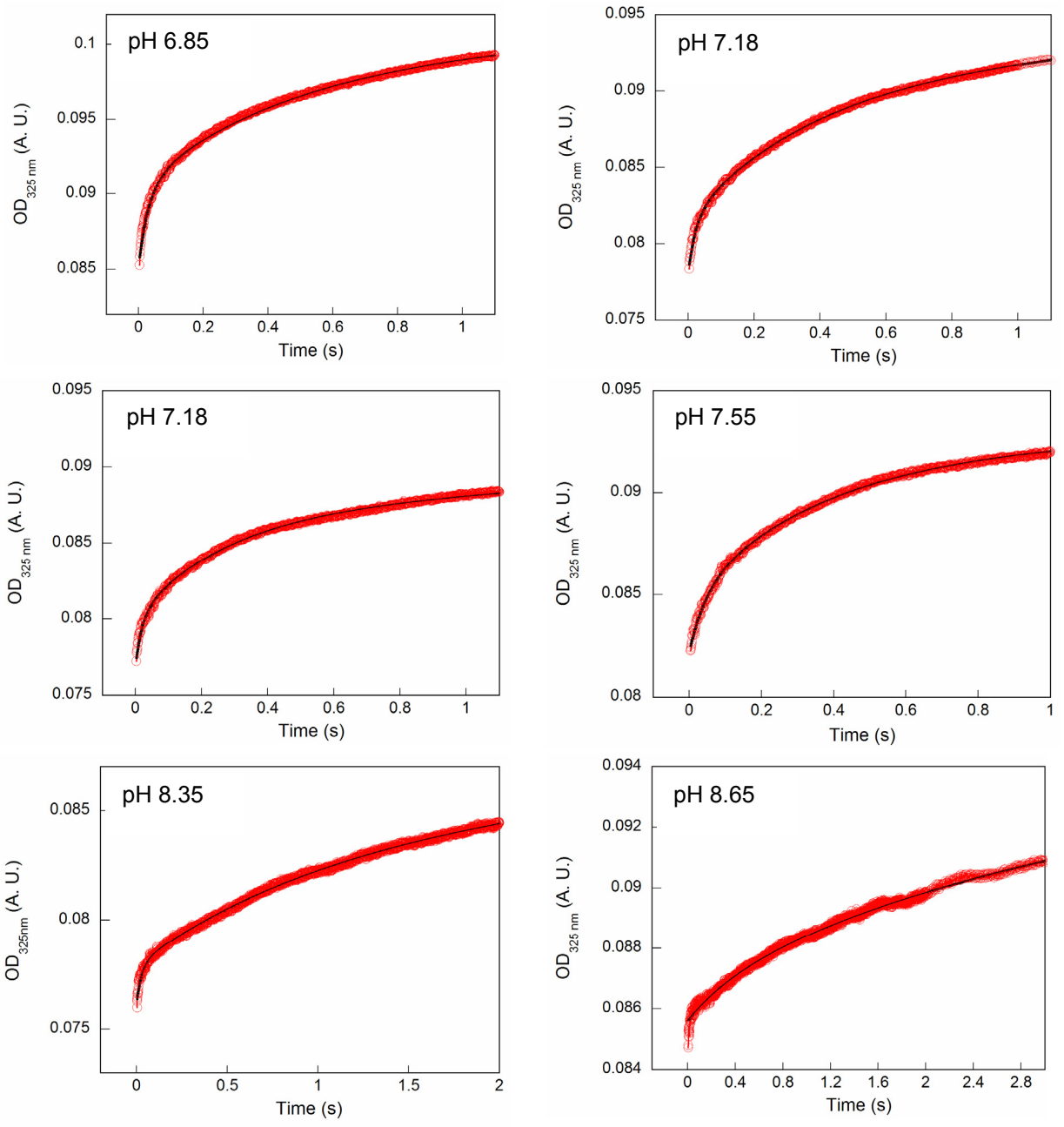

Figure S7: Magnified view of the initial 1-3 s of the SF UV-vis traces shown in Fig. 3 for the reaction of NH_2Y_{730}-α2 with F_3Y_{356}-β2 in the presence of CDP/ATP.

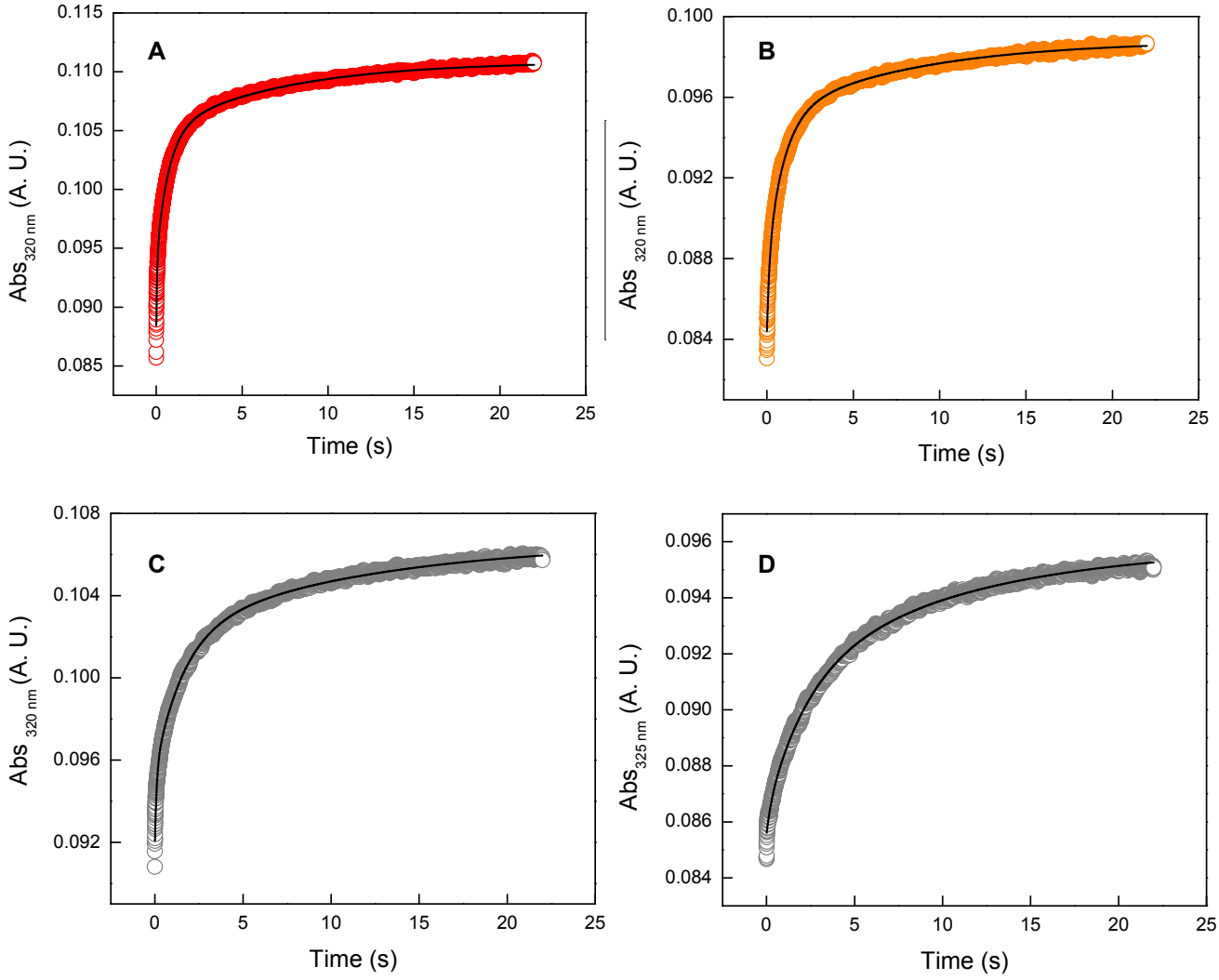

Figure S8: SF UV-vis reactions of NH_2Y_{731}-α2 with F_3Y_{356}-β2 in the presence of CDP/ATP monitored over 22 s at pH 6.6 (A), 8.45 (B) and 8.60 (C). SF UV-vis reaction of NH_2Y_{730}-α2 with F_3Y_{356}-β2 in the presence of CDP/ATP monitored over 22 s at pH 8.65 (D).

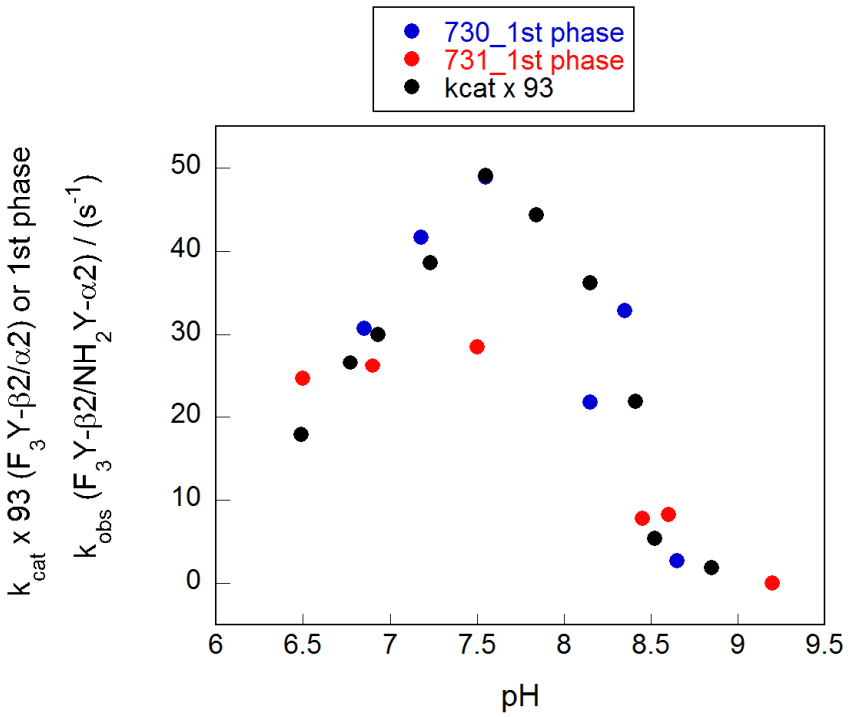

Figure S9: Comparison of the pH rate profiles from the first kinetic phase of NH_2Y• formation vs. steady state dCDP formation. Here, the k_{cat} from the reaction of F_3Y-β2 and wt α2 (black dots) has been multiplied by 93 to align the activity point at pH 7.6 and overlaid with the fast phase rate constant (see Fig. 4A) in the reaction of F_3Y-β2 with NH_2Y_{730}-α2 (blue dots) or NH_2Y_{731}-α2 (red dots).